MECHANICAL ERROR ANALYSIS OF GRATING-BASED X-RAY PHASE-CONTRAST IMAGING

[1]FAIZ WALI, [2]KUN GAO, [3]ZHAO WU, [4]WENBIN WEI, [5]PEIPING ZHU, [6]YANGCHAO TIAN1

[1,2,3,4,6]National Synchrotron Radiation Laboratory, University of Science and Technology of China, Hefei, Anhui, China, 230029, [5]Institute of High Energy Physics, Chinese Academy of Sciences, Beijing, China, 100049
E-mail: [2]gaokun@ustc.edu.cn, [3]zhupp@ihep.ac.cn, [6]ychtian@ustc.edu.cn

Abstract - Grating-based x-ray phase-contrast imaging has attracted increasing attention in recent decades. Regarding practical applications, efforts have been made to develop information extraction methods. In this work, we report quantitative descriptions of grating-based phase-contrast imaging for the mechanical error of different combination information using angular signal radiography. Results show the quality of image in different combination information of grating-based x-ray phase-contrast imaging. Our conclusions provide directions to use grating interferometer for specific and targeted applications.

Index Terms - Angular signal radiography, multi combination information, refraction, signal-to-noise ratio

I. INTRODUCTION

X-ray grating interferometer (XGI) provides phase-shift and scattering information along with absorption information about object in the beam path [1]. Therefore, for better soft tissue contrast this technique is promising imaging modality in medical imaging [1]-[7] and nondestructive testing [4]. Nonetheless, XGI [4], [8] setup is sensitive to mechanical inaccuracies, thermal effects and vibrations[9], [10]. However, extraction methods are important to minimize radiation dose, enhance image quality, high efficiency and fast acquisition. In this connection, several extraction methods have been developed to extract and separate information from projection images. Among extraction methods, phase-stepping (PS) method [11] is routinely used. However, discontinuous mod of PS restricts its clinical applications. On the other side, reverse projection (RP) method[12] is simple, fast and need low dose, but can not extract scattering signal. A newly established extraction method, so-called angular signal radiography (ASR) method [13] has reduced over all dose and improved image acquisition speed.Noise being an important figure of merit in imaging systems has been studied for PS [14]-[16], RP [17] and ASR [18] method. In our previous work [18], the signal-to-noise ratios (SNRs) of three signals (absorption, refraction and scattering) has been quantitatively evaluated and verified by simulations. In this work, SNRs of multi combination information (MCI) produced by ASR are quantitatively analyzed and validated by simulations. Mechanical error, one of the major sources of noise is analyzed by using error propagation formula [19]. MCI are used to evaluate SNRs, as for specific and targeted applications absorption, refraction and/or scattering or their combination may provide complementary information. Hence, our calculations would be useful in targeted applications where absorption, refraction and/or scattering image or their combination (s) is/are required. Our results present guidelines to enhance image quality for targeted practical applications of XGI.

II. PRINCIPLE OF ANGULAR SIGNAL RADIOGRAPHY METHOD

Classically detected image is the convolution of angle modulated function (related to object properties) and angular signal response function (shows relationship of detected intensity in XGI via x-ray deviation angle) [13]. Grating-based Talbot interferometer schematic setup is shown in Fig. 1 (a). The variation in detected intensity as function of x_g is called shifting curve (SC) and is shown in Fig. 1 (b). Angular deviation (x_g / D) is produced in XGI by relative displacement between phase grating and absorption grating. Hence, angular signal response function is substituted by SC. The details of XGI can be read in [11], [13].In ASR imaging data is investigated for four typical sections namely valley-SC (V), upslope-SC (U), peak-SC (P) and downslope-SC (D) as shown in Fig. 1 (b). The periodic intensity pattern changes when object is put in x-ray path, then the four typical imaging equations can be expressed as [13]:

$$I^s(x,y,x_g) = I_0 \bar{S} e^{-M(x,y)} \left[1 - V(x,y) \sin\left(\varphi(x,y) + \frac{2\pi}{p_2} x_g \right) \right], \quad (1)$$

Where $V(x,y) = V_0 e^{-2\pi^2 D^2 \upsilon_s^2(x,y)/p_2^2}$ and $\varphi(x,y) = \frac{2\pi D}{p_2}\left(\theta(x,y) + \psi_0\right)$. Here, $M(x,y)$, $\theta(x,y)$, $\upsilon_s^2(x,y)$, I_0 and ψ_0 are absorption, refraction angle, scattering variance of sample, intensity of incident x-ray beam and initial x-ray deviation angle respectively. $\bar{S}$ is mean value and V_0 visibility of background SC. Where D is distance

between phase and absorption grating and p_2 is period of absorption grating. Where $x_g = p_2/4, p_2/2, 3p_2/4, p_2$ corresponds to $I_V(x,y), I_U(x,y), I_P(x,y), I_D(x,y)$ respectively.

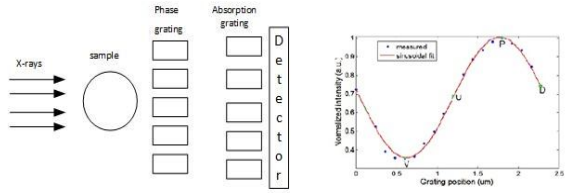


Fig. 1. (Color online) (a) Schematic setup of X-ray grating interferometer (b) plot of SC vs. function of grating position

To eliminate ψ_0, the effective absorption, refraction angle and scattering variance of sample is calculated with and without object on four typical points on SC. Hence, absorption, refraction and scattering information is extracted as: (for simplicity (x,y) is omitted).

$$M = \ln\left[\frac{I_V^b + I_U^b + I_P^b + I_D^b}{I_V^s + I_U^s + I_P^s + I_D^s}\right], \quad (2)$$

$$\theta = -\frac{p_2}{2\pi D}\left[\arctan\left(\frac{I_U^s - I_D^s}{I_V^s - I_P^s}\right) - \arctan\left(\frac{I_U^b - I_D^b}{I_V^b - I_P^b}\right)\right], \quad (3)$$

$$\upsilon_s^2 = -\frac{p_2^2}{2\pi^2 D^2}\left[\ln\left\{\frac{1}{V_0}\sqrt{\left(\frac{I_U^s - I_D^s}{I_U^b + I_D^b}\right)^2 + \left(\frac{I_V^s - I_P^s}{I_V^b + I_P^b}\right)^2}\right\} - \ln\left\{\frac{1}{V_0}\sqrt{\left(\frac{I_U^b - I_D^b}{I_U^b + I_D^b}\right)^2 + \left(\frac{I_V^b - I_P^b}{I_V^b + I_P^b}\right)^2}\right\}\right], \quad (4)$$

where I_V^b, I_U^b, I_P^b and I_D^b are background images (without sample) while I_V^s, I_U^s, I_P^s and I_D^s are sample images at four typical positions (V, U, P, D) of SC. If scattering information is neglected in ASR (NS-ASR), then by using up-slope and down-slope image, absorption and refraction can be extracted. When absorption is negligible (NA-ASR) then refraction and scattering information can be calculated by using up-slope and peak-slope image. When absorption and scattering is negligible (NANS-ASR) then refraction information can be calculated by using up-slope or down-slope image. The expressions of MCI are given in Table I.

Table I. Expressions of different combination information

	Expressions of information extraction
NS-ASR	$M_{NS} = \ln\left[\frac{I_U^b + I_D^b}{I_U^s + I_D^s}\right]$
	$\theta_{NS} = \frac{p}{2\pi D}\left[\arcsin\left(\frac{1}{V_0}\frac{I_D^s - I_U^s}{I_D^s + I_U^s}\right) - \arcsin\left(\frac{1}{V_0}\frac{I_D^b -}{I_D^b +}\right.\right.$
NA-ASR	$\theta_{NA} = \frac{p_2}{2\pi D}\left[\arctan\left(\frac{I_U^s - I_0\bar{S}}{I_P^s - I_0\bar{S}}\right) - \arctan\left(\frac{I_U^b - I_0\bar{S}}{I_P^b - I_0\bar{S}}\right)\right]$
	$\upsilon_{s,NA}^2 = \frac{p_2^2}{2\pi^2 D^2}\ln\left[\frac{\sqrt{\left(I_U^b - I_0\bar{S}\right)^2 + \left(I_P^b - I_0\bar{S}\right)^2}}{\sqrt{\left(I_U^s - I_0\bar{S}\right)^2 + \left(I_P^s - I_0\bar{S}\right)^2}}\right.$
NANS-ASR	$\theta_{NANS} = \frac{p_2}{2\pi D}\arcsin\left[\frac{I_U^s - I_0\bar{S}}{V_0 I_U^b}\right]$

Practically, one and/or two information(s) are required for specific applications, such as, absorption gives good contrast for high Z materials, while refraction has good soft-tissue contrast and scattering provides assessment of structural changes within a sample at sub-micron scale much smaller than spatial resolution of the imaging system[20]. Concerning targeted applications, MCI and its noise due to mechanical error is discussed in details.

III. NOISE ANALYSIS DUE TO MECHANICAL ERROR

In order to get four typical images phase or absorption gratings need to be translated. However, due to mechanical uncertainties actual position x_g is distributed around ideal position, which is described by normal distribution with standard deviation σ_{x_g}. These mechanical uncertainties are translated into sample intensity and finally into absorption, refraction and scattering information. The error propagation formula[19] can be applied on expressions given in Table I to get noise due to mechanical error the detailed expressions are given in Table II.

Table II. Expressions of SNRs of multi combination information

	Expressions of SNRs
NS-ASR	$SNR_M^{NS} = \frac{p_2 M_{NS}}{\sqrt{2}\pi V \cos\varphi \sigma_{x_g}}$
	$SNR_\theta^{NS} = \frac{\sqrt{2} D\theta_{NS}}{\sqrt{1 + V_0^2 \sin^2\varphi}\sigma_{x_g}}$
NA-ASR	$SNR_\theta^{NA} = \frac{D\theta_{NA}}{\sqrt{\sin^4\varphi + \cos^4\varphi}\sigma_{x_g}}$
	$SNR_{\upsilon_s^2}^{NA} = \left(\frac{\pi D^2}{\sqrt{2} p_2}\right)\frac{\upsilon_{s,NA}^2}{\cos\varphi \sin\varphi \sigma_{x_g}}$
NANS-ASR	$SNR_\theta^{NANS} = \frac{D\theta_{NANS}}{\sigma_{x_g}}$

IV. SIMULATION EXPERIMENTS AND DISCUSSIONS

Theoretical derivations given in Table II are verified by performing simulations based on wave optical approach using Matlab. XGI's phase ($\pi/2$ phase shift) and absorption grating have period of 4 μm and inter-grating period is set to first fractional Talbot distance, 16.13 cm. A plane wave x-ray beam of 25 keV and intensity of 10000 photons/pixel is used to get four typical images. A cylinder made up of PMMA having diameter 10 mm is used as sample. The refractive index of PMMA is $n = 1 - 4.26\times10^{-7} + i1.53\times10^{-10}$ at 25 keV. The projection images are acquired by using ASR method. Different stepping motors having precision 0.0012, 0.0014, 0.0016, 0.0018, 0.0020, 0.0022, 0.0024 are used to calculate noise. The precision of stepping motors are selected according to minimal incremental motion as explained in [14].

Fig. 2 shows simulated images and SNRs of simulation and theory in case of negligible scattering. When scattering signal is negligible then simulated absorption and refraction images obtained by ASR is shown in Fig. 2 (a) and (b) respectively. The SNRs of absorption image when scattering is negligible is shown in Fig. 2 (c). The SNRs of absorption in case of negligible scattering is directly proportional to period of absorption grating and inversely proportional to visibility. When scattering is negligible then SNRs of refraction is shown in Fig. 2 (d). The SNRs of refraction in case of negligible scattering is directly proportional to inter-grating distance. In addition, the SNRs of absorption and refraction in case of negligible scattering are inversely proportional to standard deviation.

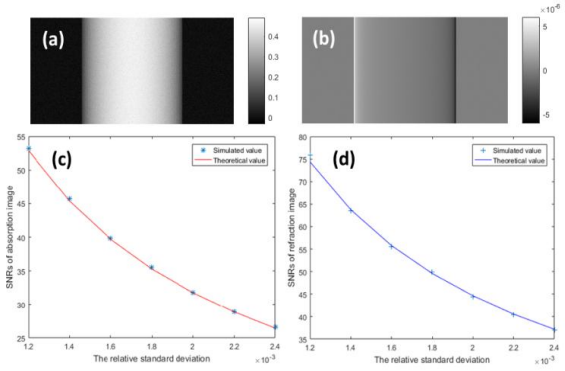


Fig. 2. Simulated images and SNRs of negligible scattering: (a) simulated absorption image (b) simulated refraction image (c) SNRs of simulation and theory for absorption image (d) SNRs of simulation and theory for refraction image

Fig. 3 (a) and (b) shows simulated refraction and scattering images respectively, while absorption is neglected. The SNRs of refraction and scattering images are shown in Fig. 3 (c) and (d) respectively, while absorption is neglected. The SNRs of both refraction and scattering images are inversely proportional to standard deviation. Moreover, SNRs of refraction of image is directly proportional to inter-grating distance while SNRs of scattering is directly proportional to square of inter-grating distance, while absorption is neglected. Here, we point out that SNRs of scattering when absorption is negligible, is inversely proportional to period of absorption grating.

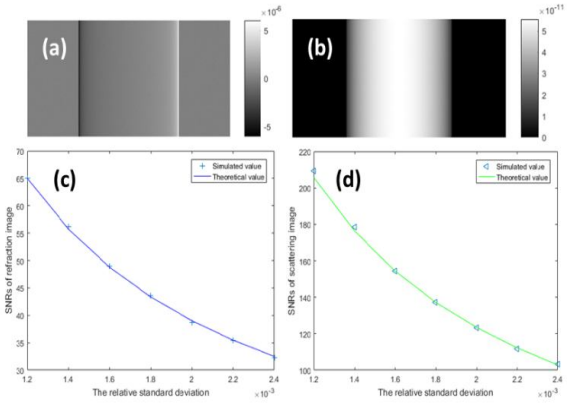


Fig. 3. (a) simulated refraction image (b) simulated scattering image (c) simulated and theoretical SNRs of refraction image (d) simulated and theoretical SNRs of scattering image in case of negligible absorption.

The simulated image of refraction image when absorption and scattering is neglected is shown in Fig. 4 (a). The simulated and theoretical result of SNRs of negligible absorption and negligible scattering is shown in Fig. 4(b). Here, we underline that SNRs of negligible absorption and negligible scattering is directly proportional to inter-grating distance and inversely proportional to standard deviation.

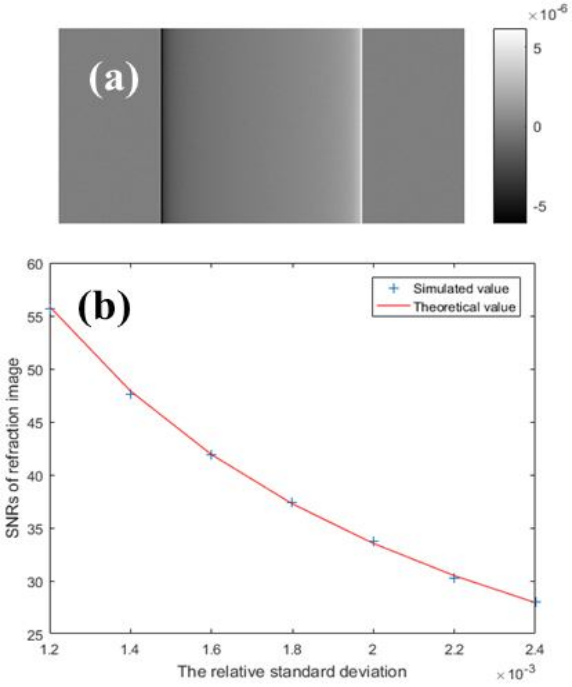


Fig. 4. SNRs of NANS

In all MCI theoretical predictions are in good agreement with simulation shown in Figs. 2 (c, d), 3 (c, d) and 4 (b), hence validates our theoretical derivations. Moreover, in all MCI the SNRs are inversely proportional to standard deviation, which is consistent with previously published reports [14, 17, 18].

CONCLUSION

SNRs of MCI due to mechanical error are theoretically derived and validated with simulation. In all MCI simulation results are in good agreement with theory. In all cases SNRs are inversely proportional to standard deviation. In addition, other factors dependence on SNRs is discussed. Finally, SNRs derivations could be applied in targeted and specific applications where high contrast images are required.

REFERENCES

[1] Li, Ke, YongshuaiGe, John Garrett, Nicholas Bevins, Joseph Zambelli, and Guang-Hong Chen. "Grating-based phase contrast tomosynthesis imaging: Proof-of-concept experimental studies." Medical physics 41, no. 1 (2014).

[2] Momose, Atsushi, Tohoru Takeda, Yuji Itai, and Keiichi Hirano. "Phase–contrast X–ray computed tomography for observing biological soft tissues." Nature medicine 2, no. 4 (1996): 473-475.

[3] Fitzgerald, Richard. "Phase-sensitive x-ray imaging." Phys. Today 53, no. 7 (2000): 23-26.

[4] Pfeiffer, Franz, TimmWeitkamp, Oliver Bunk, and Christian David. "Phase retrieval and differential phase-contrast imaging with low-brilliance X-ray sources." Nature physics 2, no. 4 (2006): 258.

[5] Stampanoni, Marco, Zhentian Wang, Thomas Thüring, Christian David, EwaldRoessl, MafaldaTrippel, Rahel A. Kubik-Huch, Gad Singer, Michael K. Hohl, and Nik Hauser. "The first analysis and clinical evaluation of native breast tissue using differential phase-contrast mammography." Investigative radiology 46, no. 12 (2011): 801-806.

[6] Michel, Thilo, Jens Rieger, Gisela Anton, Florian Bayer, Matthias W. Beckmann, Jürgen Durst, Peter A. Fasching et al. "On a dark-field signal generated by micrometer-sized calcifications in phase-contrast mammography." Physics in Medicine & Biology 58, no. 8 (2013): 2713.

[7] Bech, Martin, A. Tapfer, A. Velroyen, A. Yaroshenko, B. Pauwels, J. Hostens, P. Bruyndonckx, A. Sasov, and F. Pfeiffer. "In-vivo dark-field and phase-contrast x-ray imaging." Scientific reports 3 (2013): 3209.

[8] Momose, Atsushi, Shinya Kawamoto, Ichiro Koyama, Yoshitaka Hamaishi, KengoTakai, and Yoshio Suzuki. "Demonstration of X-ray Talbot interferometry." Japanese journal of applied physics 42, no. 7B (2003): L866.

[9] Tapfer, Arne, Martin Bech, Astrid Velroyen, Jan Meiser, Jürgen Mohr, Marco Walter, Joachim Schulz et al. "Experimental results from a preclinical X-ray phase-contrast CT scanner." Proceedings of the National Academy of Sciences 109, no. 39 (2012): 15691-15696.

[10] Koehler, Thomas, HeinerDaerr, Gerhard Martens, Norbert Kuhn, Stefan Löscher, UdoStevendaal, and EwaldRoessl. "Slit-scanning differential x-ray phase-contrast mammography: Proof-of-concept experimental studies." Medical physics 42, no. 4 (2015): 1959-1965.

[11] Weitkamp, Timm, Ana Diaz, Christian David, Franz Pfeiffer, Marco Stampanoni, Peter Cloetens, and Eric Ziegler. "X-ray phase imaging with a grating interferometer." Optics express 13, no. 16 (2005): 6296-6304.

[12] Zhu, Peiping, Kai Zhang, Zhili Wang, Yijin Liu, Xiaosong Liu, Ziyu Wu, Samuel A. McDonald, Federica Marone, and Marco Stampanoni. "Low-dose, simple, and fast grating-based X-ray phase-contrast imaging." Proceedings of the National Academy of Sciences 107, no. 31 (2010): 13576-13581.

[13] Li, Panyun, Kai Zhang, Yuan Bao, YuqiRen, ZaiqiangJu, Yan Wang, Qili He et al. "Angular signal radiography." Optics express 24, no. 6 (2016): 5829-5845.

[14] Revol, Vincent, Christian Kottler, Rolf Kaufmann, Ulrich Straumann, and Claus Urban. "Noise analysis of grating-based x-ray differential phase contrast imaging." Review of Scientific Instruments 81, no. 7 (2010): 073709.

[15] Chen, Guang-Hong, Joseph Zambelli, Ke Li, Nicholas Bevins, and Zhihua Qi. "Scaling law for noise variance and spatial resolution in differential phase contrast computed tomography." Medical physics 38, no. 2 (2011): 584-588.

[16] Weber, T., P. Bartl, J. Durst, W. Haas, T. Michel, A. Ritter, and G. Anton. "Measurements and simulations analysing the noise behaviour of grating-based X-ray phase-contrast imaging." Nuclear Instruments and Methods in Physics Research Section A: Accelerators, Spectrometers, Detectors and Associated Equipment 648 (2011): S273-S275.

[17] Wu, Z., Z. L. Wang, K. Gao, D. J. Wang, S. H. Wang, J. Chen, H. Chen, K. Zhang, P. P. Zhu, and Z. Y. Wu. "Signal-to-noise ratio analysis of X-ray grating interferometry with the reverse projection extraction method." Journal of Electron Spectroscopy and Related Phenomena 196 (2014): 75-79.

[18] Faiz, Wali, Yuan Bao, Kun Gao, Zhao Wu, Chen-Xi Wei, Gui-Bin Zan, Pei-Ping Zhu, and Yang-Chao Tian. "Noise analysis of grating-based x-ray differential phase-contrast imaging with angular signal radiography." Chinese Physics B 26, no. 4 (2017): 040602.

[19] BRONSHTEIN I N, SEMENDYAYEV K A F. Handbook of Mathematics [M]. Springer Science & Business Media, 2013.

[20] Von Teuffenbach, Maximilian, Thomas Koehler, Andreas Fehringer, Manuel Viermetz, Bernhard Brendel, Julia Herzen, Roland Proksa, Ernst J. Rummeny, Franz Pfeiffer, and Peter B. Noël. "Grating-based phase-contrast and dark-field computed tomography: a single-shot method." Scientific reports 7, no. 1 (2017): 7476.

★★★